

Model Calculation of Stress-Strain Relationship of Polycrystalline Fe-Pd and 3D Phase Transformation Diagram of Ferromagnetic Shape Memory Alloys

Yuanchang Liang^a, Taishi Wada^a, Tetsuya Tagawa^b, M. Taya^a

^aCenter for Intelligent Materials and Systems, Dept. of Mechanical Engineering,
University of Washington, Seattle, WA 98195-2600, USA

^bDept. of Material Science and Engineering, Nagoya University, Japan

ABSTRACT

A micromechanics approach is proposed to calculate the stress-strain relationship of a polycrystalline Fe-Pd ferromagnetic shape memory alloy. It is modeled as consisting of spherical grains, which are grouped according to their orientations with respect to the loading axis. Therefore, the internal stress and elastic energy are accumulated as straining proceeds due to the strain differences between differently oriented grains. In the present study, the energy dissipation of the interface movement is also considered. Furthermore, a stress-magnetic field-temperature phase transformation diagram is constructed. The magnetic field induced transformation is found to be insignificant based on thermodynamics model. The cases of Fe-Pd and NiMnGa systems are examined for 3D phase transformation diagram.

Keywords: phase diagram, shape memory alloy, ferromagnetic, Fe-Pd, stress-strain relationship

1. INTRODUCTION

Fe-Pd, a ferromagnetic shape memory alloy (FSMA), has attracted a strong attention because it has a potential for use as a magnetic field-controlled and robust actuator material, which has fast responsive actuation with large stroke and force capability. Because of its ductile property, Fe-Pd alloy can be mechanically worked into different shapes¹. It is noted that another FSMA, NiMnGa alloy is much more difficult in processing. Among possible magnetic field-actuation mechanisms¹⁻⁵, the hybrid mechanism^{1,2}, stress-induced martensitic transformation caused by the force due to the magnetic field gradient, seems to be superior to other mechanisms. Thus, the modeling of stress-strain relationship of polycrystalline Fe-Pd and its phase diagram become important for design of robust actuators.

As reported previously, polycrystalline Fe-Pd has low stiffness in the martensite state⁶. In addition to intrinsically low lattice stiffness, large strains are developed upon loading due to changes in martensite variant fractions. This makes polycrystalline Fe-Pd softer material, suitable for certain actuator applications. The structure of martensite in a polycrystal of Fe-Pd has been analyzed⁷. Three Bain correspondence variants of tetragonal martensite, BCV(1), BCV(2) and BCV(3), exist in Fe-Pd. When formed by cooling, a grain has a structure consisting of alternating dark and bright plates, as observed under optical microscopy⁷. The width of the plates is a few μm . Each plate has a fine structure where two twin-related BCVs are alternately stacked together. A BCV is about 50nm thick. The fractions of BCVs change by movement of the interfaces due to external loading, resulting in straining of the polycrystal. The variant change depends on the orientation of a grain and the constraint imposed by the surrounding grains. Since polycrystalline Fe-Pd is likely to be used for actuator applications, the determination of stress-strain relationship is a key engineering issue.

The phase transformation temperatures of shape memory alloys (SMAs) can be changed by external loading. The stress-temperature phase transformation diagram is usually used to show this relationship. This diagram is also important in view of designing actuators based on SMAs. Similarly, the stress-temperature phase transformation diagram can be extended to a stress-magnetic field-temperature phase transformation diagram for FSMAs which have both martensitic transformation and ferromagnetic properties. In the present, this phase diagram is called three dimensional phase transformation diagram.

This paper presents a method to calculate the above mentioned variant change and straining under uniaxial loading of polycrystalline Fe-Pd, using the mean field method^{8,9}, and discuss the analytical model based on thermodynamics and ferromagnetism to construct 3D phase transformation diagram.

2. ANALYSIS

2.1 Straining of fully martensite structure

The average transformation strain⁷ (eigenstrain) in a Fe-Pd grain can be written as

$$\varepsilon^*(\mathbf{Y}) = \frac{2\varepsilon_a + \varepsilon_c}{3} \begin{pmatrix} 1 & 0 & 0 \\ 0 & 1 & 0 \\ 0 & 0 & 1 \end{pmatrix} - (\varepsilon_a - \varepsilon_c) \begin{pmatrix} f_1 - 1/3 & 0 & 0 \\ 0 & f_2 - 1/3 & 0 \\ 0 & 0 & f_3 - 1/3 \end{pmatrix}. \quad (1)$$

Here, f_1 , f_2 and f_3 are the volume fraction of BCV(1), BCV(2) and BCV(3), respectively. The eigenstrain in Eq.(1) refers to the coordinate system (Y) with axes parallel to the crystallographic directions, [100], [010] and [001], in the austenite. The first term in Eq.(1) is common among all grains and causes no internal stress. Thus, it is omitted in the following analysis. The second term is rewritten as

$$\varepsilon^*(\mathbf{Y}) = -\beta \begin{pmatrix} f_1^* & 0 & 0 \\ 0 & f_2^* & 0 \\ 0 & 0 & f_3^* \end{pmatrix}, \quad (2)$$

where

$$\beta = \varepsilon_a - \varepsilon_c, \quad (3)$$

and

$$f_1^* = f_1 - 1/3, \quad f_2^* = f_2 - 1/3, \quad f_3^* = f_3 - 1/3. \quad (4)$$

Note that f_i^* satisfy

$$f_1^* + f_2^* + f_3^* = 0. \quad (5)$$

Then, the task here is to evaluate the internal stresses and elastic energy in polycrystalline Fe-Pd, in which many differently oriented grains exist and undergo variant changes depending on their orientations. Considering the case of uniaxial loading, the specimen coordinate reference frame is denoted as x_1, x_2, x_3 being parallel to the loading direction. To facilitate the calculation, the grains are grouped into N groups. All grains belonging to the same group, say the I-th group, have the same crystallographic direction along the loading direction. This direction has a unit vector $l(I)$ with the assumption that grains having the same direction along the loading axis are present axisymmetrically with respect to the loading direction. A polycrystal which possesses grains having many different orientations $l(I)$ is randomly oriented. The stable condition of a specimen by a uniaxial loading is found when Gibbs free energy is minimized (ignoring the energy dissipation)

$$\delta(W+V) = 0, \quad (6)$$

where W is the elastic energy (per unit volume) and V is the potential energy (per unit volume) of the loading device. W is calculated as¹⁰

$$W = -\frac{1}{2} \sum_I g(I) \{ \sigma_{ij}^*(I) + \bar{\sigma}_{ij} \} \varepsilon_{ij}^*(I) , \quad (7)$$

where I is the I-th group of grains. The first term is the self-energies of all the grains and is calculated using the components expressed in the crystal coordinates (Y-coordinate) where the stress in a grain belonging to the I-th group is written as

$$\sigma^*(I, Y) = \alpha \beta \begin{pmatrix} f_1^*(I) & 0 & 0 \\ 0 & f_2^*(I) & 0 \\ 0 & 0 & f_3^*(I) \end{pmatrix} \quad (8)$$

when only this grain changes its variant fractions¹¹. Here, α is

$$\alpha = 2\mu \frac{(7-5\nu)}{15(1-\nu)} . \quad (9)$$

The shape of a grain is assumed to be spherical. μ is the shear modulus and ν the Poisson ratio of austenite. Isotropic elasticity is assumed. $\sigma^*(I, Y)$ is called the self-stress of a grain in the I-th group.

The second term in Eq.(7) is the interaction energy between the grains calculated using the components in the specimen X-coordinates. To calculate this internal stress, the following procedures are used. Equation (2) is written in the specimen coordinate (X-coordinate system) as

$$\varepsilon^*(I, X) = -\beta \begin{pmatrix} \lambda_1(I) & \varepsilon_{12}^*(I) & \varepsilon_{13}^*(I) \\ \varepsilon_{21}^*(I) & \lambda_2(I) & \varepsilon_{23}^*(I) \\ \varepsilon_{31}^*(I) & \varepsilon_{32}^*(I) & \lambda_3(I) \end{pmatrix} , \quad (10)$$

and the stress field by this eigenstrain is given by¹¹

$$\sigma^*(I, X) = \alpha \beta \begin{pmatrix} \lambda_1(I) & \varepsilon_{12}^*(I) & \varepsilon_{13}^*(I) \\ \varepsilon_{21}^*(I) & \lambda_2(I) & \varepsilon_{23}^*(I) \\ \varepsilon_{31}^*(I) & \varepsilon_{32}^*(I) & \lambda_3(I) \end{pmatrix} . \quad (11)$$

Here,

$$\lambda_3(I) = f_1^*(I)(l_1(I))^2 + f_2^*(I)(l_2(I))^2 + f_3^*(I)(l_3(I))^2 , \quad (12)$$

$$\lambda_1(I) + \lambda_2(I) + \lambda_3(I) = 0 . \quad (13)$$

λ_3 is the tensile strain along this direction. $\varepsilon_{12}(I)$ etc depend on $f_1^*(I)$, $f_2^*(I)$ and $f_3^*(I)$ and the exact orientation of the grain with respect to the loading direction.

Stress in Eq.(11) is averaged over all the grains of the I-th group. Because of the axi-symmetry around the x_3 -axis, the averages of the stresses due to the non-diagonal components in Eq.(11) vanish and the averages of the {1,1} and {2,2} components become the average of those components in Eq.(11). In this way, the average stress can be calculated as

$$\langle \sigma^*(\mathbf{I}, \mathbf{X}) \rangle_{v_0} = \alpha\beta \begin{pmatrix} -\lambda_3(\mathbf{I})/2 & 0 & 0 \\ 0 & -\lambda_3(\mathbf{I})/2 & 0 \\ 0 & 0 & \lambda_3(\mathbf{I}) \end{pmatrix}. \quad (14)$$

Here, v_0 stands for the volume of one grain. The grain in the I-th group cause average stress in the specimen given by^{8,9}

$$\bar{\sigma}(\mathbf{I}, \mathbf{X}) = -g(\mathbf{I}) \langle \sigma^*(\mathbf{I}, \mathbf{X}) \rangle_{v_0}. \quad (15)$$

Here $g(\mathbf{I})$ is the volume fraction of the grains belonging to the I-th group.

Similar equations are written for grains belonging to other groups. Thus, one grain belonging to the I-th group feels its self-stress plus the average stress from all other grains. The average stress is the sum of the forms given by Eq.(15) over all the groups. That is, the average stress is, in total,

$$\bar{\sigma}(\mathbf{X}) = -\sum_{\mathbf{J}} g(\mathbf{J}) \langle \sigma^*(\mathbf{J}, \mathbf{X}) \rangle_{v_0}. \quad (16)$$

The potential energy, V , of the loading device is written as

$$V = -\sigma_0 \varepsilon, \quad (17)$$

where σ_0 is the uniaxial stress along the loading direction and the strain, ε , in the specimen X-coordinates along the loading direction on x_3 -axis is given by Eqs. (10) and (12) as

$$\varepsilon = -\beta \sum_{\mathbf{I}} g(\mathbf{I}) \{ f_1^*(\mathbf{I})(l_1(\mathbf{I}))^2 + f_2^*(\mathbf{I})(l_2(\mathbf{I}))^2 + f_3^*(\mathbf{I})(l_3(\mathbf{I}))^2 \}, \quad (18)$$

where only {3,3} component in Eq.(10) exists under this loading direction.

Then, Eq.(6) results in a set of simultaneous linear equations in terms of $f_1^*(\mathbf{I})$, $f_2^*(\mathbf{I})$ and $f_3^*(\mathbf{I})$. Thus, all of $f_1^*(\mathbf{I})$, $f_2^*(\mathbf{I})$ and $f_3^*(\mathbf{I})$ are, in principle, solved analytically as a function of the uniaxial stress σ_0 under the constraint of Eq.(5). Furthermore, $f_1^*(\mathbf{I})$, $f_2^*(\mathbf{I})$ and $f_3^*(\mathbf{I})$ must satisfy

$$-1/3 \leq f_1^*, f_2^*, f_3^* \leq 2/3. \quad (19)$$

Using Eq.(18), the strain ε along the loading direction attained under a uniaxial stress σ_0 is also obtained. Thus, the σ_0 vs ε relationship is computed. Since energy dissipation is ignored, the variant change and the accompanied deformation proceed from $\sigma_0 = 0$. This is unrealistic, thus, the energy dissipation is now taken into account in the next section

2.2 Effect of Energy Dissipation on the Movement of Interfaces

Changes in the fractions of the martensite variants are produced by the movement of interfaces between them. Movement of the interfaces dissipates energy. Thus, extra work is supplied for straining. The energy dissipation will be approximately evaluated and incorporated into the stress-strain relationship. The present study proposes that the energy dissipation is calculated approximately as

$$\delta W_D = k \left(|\delta f_1^*| + |\delta f_2^*| + |\delta f_3^*| \right) / 2 \quad (20)$$

per unit volume. k is the energy dissipation when a unit area of interface moves by a unit distance. The factor 2 is introduced to account for the fact that the movement of an interface changes the volumes of both variants which meet at the interface. Since this process is irreversible, the energy minimization procedure can not be used to obtain the σ_0 vs ε relationship as adopted for the case of no energy dissipation. Thus, we can simply add

$$\sigma_D = \delta W_D / \delta \varepsilon \quad (21)$$

to σ_0 which was determined without considering the energy dissipation. Here, $\delta \varepsilon$ is the increment of ε for the same change in the variant fractions. Since there is no unique way to determine k , the value, which gives the initial stress for variant change observed in the previous study, is adopted. The following will show using a dislocation approach that the order of magnitude is correct.

Since two adjoining BCVs match perfectly on their interface, the movement is caused by the nucleation of a dislocation loop on the interface and its subsequent spreading-out. Apparently, the nucleation is the rate controlling process. The energy change when a dislocation loop is formed (Gibbs free energy assigned for the loop), is approximately written as

$$G = 2\pi r \frac{1}{2} \mu b^2 - \sigma_0 \pi r^2 b, \quad (22)$$

where b is the Burgers vector of the dislocation and r the radius of the loop. The condition for the maximum of G (activation energy) is calculated as

$$\frac{\partial G}{\partial r} = 0, \quad r^* = \frac{\mu b}{2\sigma_0}. \quad (23)$$

Therefore, the maximum G , G^* is obtained as

$$G^* = \pi \mu^2 b^3 / (4\sigma_0). \quad (24)$$

As often used in dislocation dynamics, such a process occurs with an observable rate, when

$$G^* = 26 K_B T, \quad (25)$$

where k_B is the Boltzmann constant and T the absolute temperature¹². b in this case is in the order of $a_0(\varepsilon_a - \varepsilon_c)$ (a_0 is taken as the lattice parameter of the austenite). Using $T = 300\text{K}$, $\mu = 15\text{GPa}$ ⁶ and $(\varepsilon_a - \varepsilon_c) = 2.54 \times 10^{-2}$ (based on the lattice parameters reported by Oshima¹³: $a_0 = 0.3750\text{nm}$, $a = 0.3790\text{nm}$ and $c = 0.3695\text{nm}$), Eqs. (24) and (25) give

$$\sigma_0 = 1.4 \text{ MPa} \quad (26)$$

as the stress for the interface movement.

An interface which is not perfectly flat in the beginning contains steps. The steps are dislocations as discussed here. When they move, they eventually disappear at a specimen surface or a grain boundary or annihilate each other. This process leads to micro-straining. After this process, an interface becomes flat. Long distance movement of a variant interface, leading to large strain, requires the process discussed in the above paragraph. Since flat interfaces are crystallographically fixed, one cannot control the mobility of the interfaces for long distance movement as one wishes. Usual grain boundaries do not play any role in this movement.

The stress-strain diagrams with and without the energy dissipation are compared as shown in Fig.1. The diagram shows the case of four types of grains, the tensile directions of which are shown on the standard stereographic triangle in the insert. Each group of grains has volume fraction proportional to the solid angle indicated by its small triangle. In the computation, $\mu = 15\text{GPa}^6$, $\nu = 0.33$ and $k = 2\text{MPa}$ are assumed. Also, $\beta = \epsilon_a - \epsilon_c = 2.54 \times 10^{-2}$ is used¹³. As expected, the energy dissipation just simply increases the stress level. Except for this change, no significant effect of the dissipation is seen in the σ_0 vs ϵ curve. After an initial low gradient stage, the stress increases sharply as the strain approaches a limiting value. For reference, largest stress attained can be estimated as $8 \times 10^3 \text{MPa}$ in the 4 grain problem. The limiting (maximum) strain is about 0.27β in tension and about -0.37β in compression for Fe-Pd system.

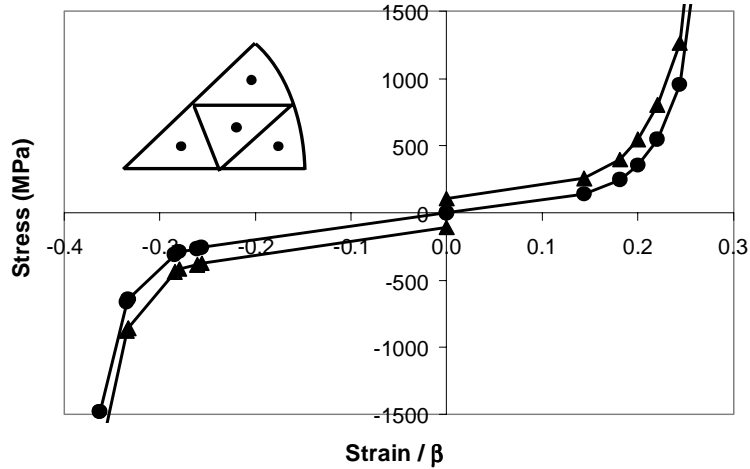


Figure 1 Stress-strain curves of a polycrystalline Fe-Pd having 4 types of grains with (closed triangle) and without (closed circle) energy dissipation ($k = 2\text{MPa}$).

2.3 Discussion

The stress in the last stage becomes larger because grains having the orientation near $\langle 111 \rangle$ are introduced. However, the large stress region near the end of complete variant change should not be emphasized so strongly. In reality, such large stress induces plastic deformation by dislocation movement, prior to the completion of the variant change. The plastic deformation obscures the sharp rise in stress predicted theoretically in the present study.

Next, it should be mentioned why the elastic energy is concisely described by Eq.(7) including the interaction energy term. This is simply due to the assumption that grains having the same direction along the loading axis are present axisymmetrically with respect to the loading direction. Otherwise, such a simple expression of Eq.(14) cannot be obtained for calculating the interaction energy in Eq.(7). An example of non-axisymmetric texture is a material having a sheet or plate texture. If a material has a fiber texture (axisymmetric texture), the present method results in an equally simple formulation of energy and the pre-determination of $l(I)$ and $g(I)$ in the fiber textures is all that is required to find the σ_0 vs ϵ relationship.

The structure of martensite formed by stressing is different from that formed by cooling. By cooling, dark and bright plates coexist in a grain in equal amounts. By stressing, only one type of plates appears⁶. As stress is increased, this one type of plates increases in number and width and eventually a whole grain becomes monotoned. From this observation, a model can be made. (1) in the first stage, identical twin plates (TWP) consisting of two BCVs are formed in a grain. (2) In the second stage, the fractions of the two BCVs in grain change, until a whole grain is covered by a single BCV. The present study is working well for strain limited to a small value but not for larger strain. The elastic energy (W) and the potential energy (V) of a loading device are continuous at the strain where f becomes one and f_1 and f_2 start to change from the prefixed value, $f_1 = \epsilon_a / (\epsilon_a - \epsilon_c)$. However, their derivatives, for example, ϵ is not. This is seen easily by checking the derivative of V . When $f \leq 1$, V is proportional to f , while $f \geq 1$, V does not depend on f . This is the origin

of the discontinuity. Of course, this is caused by the approximation: the fractions of constituting twins are constant until f becomes one. Strictly speaking, this constant structure is not assured where the fractions of BCVs would presumably change during loading or loading¹. Therefore, the change of BCV fractions should be taken into account.

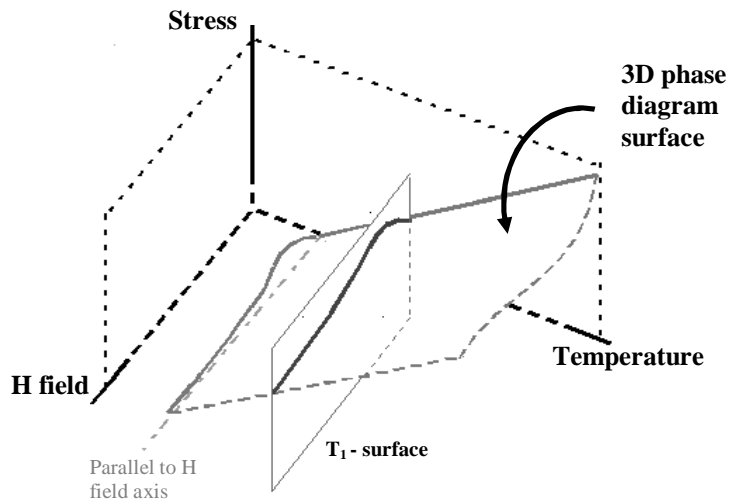


Figure 2 The stress-magnetic field – temperature phase diagram of Fe-Pd FSMA

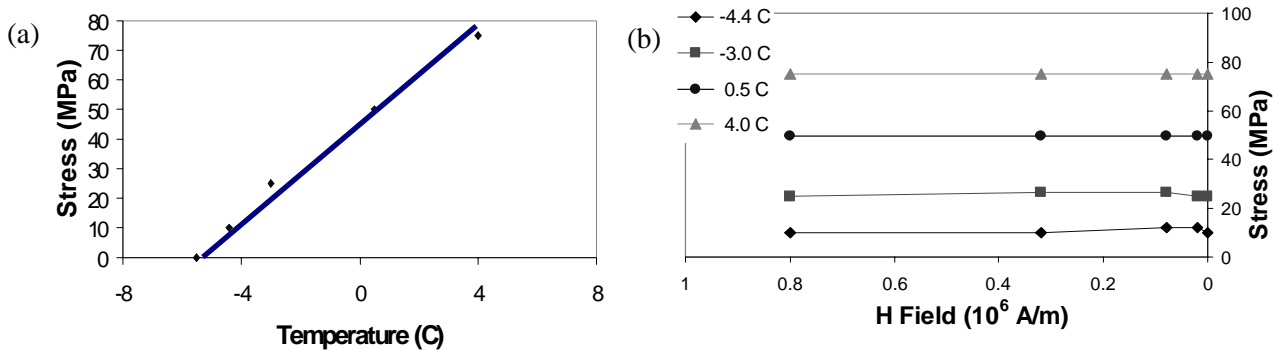


Figure 3 (a) The stress- temperature phase diagram of Fe-Pd FSMA, (b) the stress-magnetic field phase diagram under several temperatures

3. PHASE DIAGRAM

Figure 2 shows the over view of the stress-magnetic field-temperature phase transformation diagram for polycrystalline Fe-Pd. To construct the stress-temperature phase transformation diagram, the Fe-Pd specimen is loaded uniaxially by an Instron machine and it is insulated by a quartz tube for ensuring uniform temperature. Figure 3(a) shows the stress-temperature phase transformation diagram measured experimentally. The curve clearly show that the larger stress applied, the higher transformation temperature is. The slop of the curve is similar to the previous result⁶ which was also confirmed by the Clapeyron-Clausius relationship. During the loading, a magnetic field can be applied simultaneously to the specimen in the transverse direction. Therefore, the effect of both stress and magnetic field on the transformation is present by the stress-magnetic field diagram as shown in Fig.3(b). It clearly shows that the curves almost parallel to the magnetic field axes. This implies that the shift of the transformation temperature by magnetic field is very small while the temperature shifted by stress is very significant. Therefore, the small magnetic field effect on the phase transformation is evidenced in the three dimensional phase transformation diagram as the H-T phase boundary surface is nearly parallel to the magnetic field axis as shown in Fig.4. This is conducted by an examination of the martensitic transformation based on the differential thermal analysis (DTA) measurement under a given magnetic field. The curve

slightly inclines to the magnet field axis. This means the magnetic field has a small negative effect on the martensitic transformation which is also conformed by microscopic observations.

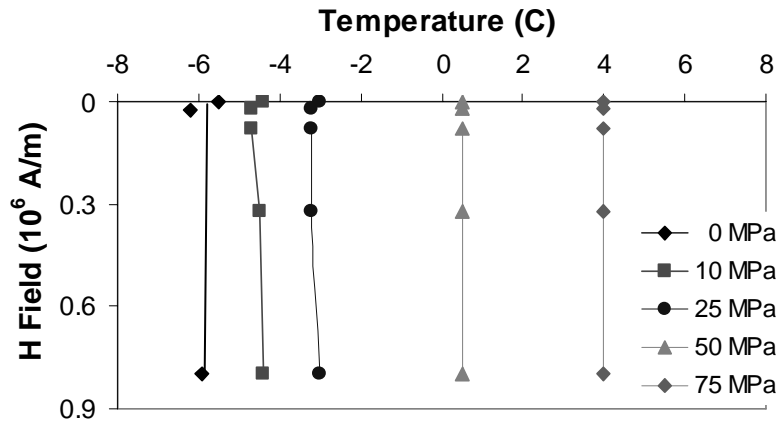


Figure 4 The magnetic fields-temperature phase diagram of Fe-Pd FSMA

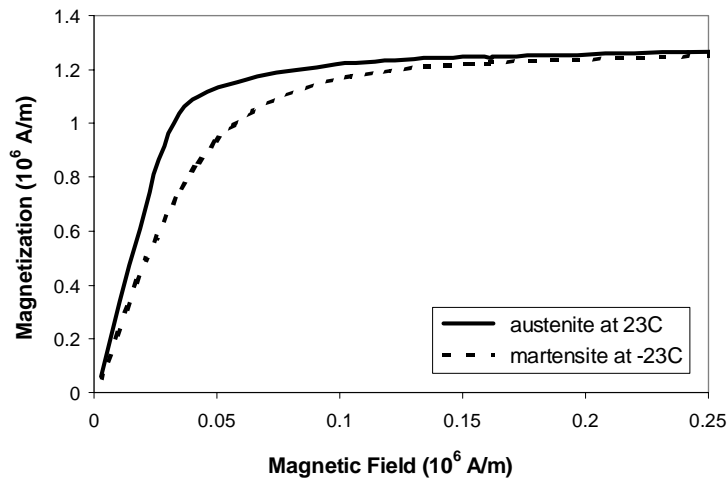


Figure 5 The magnetization curves of Fe-Pd FSMA in austenite phase and martensite phase

The freshly formed martensite plates by cooling disappear upon the application of 8×10^5 A/m field. Immediately upon the removal of the field, the identical martensite plates reappear. This means that the transformation temperature of those martensite plates is lowered by a magnetic field. The Clapeyron-Clausius equation gives a change of the transformation temperature in this case as

$$\Delta T = \frac{T}{L} \int_0^{H_M} \Delta M dH, \quad (27)$$

where T is the transformation temperature under no magnetic field, L the enthalpy change in the transformation from austenite to martensite, ΔM the magnetization change in the transformation and H_M the maximum magnetic field applied. Graphically integrating Fig. 5. with $H_M = 8 \times 10^5$ A/m and using $L = 0.42 \times 10^7$ J/m³, $\Delta T = -1.3^\circ\text{C}$ can be obtained from Eq.(27). This is an overestimate, as will be discussed below, but can explain the disappearance of freshly formed

martensite plates by the application of a magnetic field. As seen from Fig. 5, the contribution of ΔM to the integral in Eq.(27) is most significant when H is small, where a difference in the magnetization between austenite and martensite is large. In this case, a difference in the magnetization is smaller and, thus, the magnitude of ΔT must become smaller than 1.3°C which is calculated, using the magnetization at -23°C , Fig. 5. This temperature is significantly lower than the transformation temperature, 0°C , and a difference in the magnetization between austenite and martensite is larger than that near 0°C . Thus, the calculation based on Fig. 5 and use of -23°C overestimates the magnitude of ΔT . This explains that only some freshly formed martensite plates are affected by the magnetic field. The fact of negative temperature change ($\Delta T < 0$) in the above is consistent with the DTA measurement and the experimental observation of disappearance in some of the martensite plates in Fe-Pd subjected to applied magnetic field.

Note that the direct effect of magnetic field on the transformation of Fe-Pd alloy is to promote the reverse transformation (martensite \rightarrow austenite). However, for the case of NiMnGa, it is opposite. This difference is shown in Fig. 6 and can be explained based on the magnetization. Since the saturated magnetization (M_s) of Fe-Pd austenite phase is similar to that of martensite phase, the applied magnetic field tends to retard the forward transformation. However, the M_s of NiMnGa martensite phase has been reported larger than that of austenite phase^{14,15}. Therefore, the applied magnetic field tends to promote the forward transformation in NiMnGa. Of course, the direct magnetic field effect for both cases are very small: less than 1°C change of transformation temperature under $8 \times 10^5 \text{ A/m}$. The transformation changed by applied magnetic field can be described by thermal dynamics analysis. In Eq.(27), $\Delta M = M_M - M_A$ means the magnetization difference between martensite and austenite. In the case of NiMnGa, ΔM is positive under magnetic field of $8 \times 10^5 \text{ A/m}$. This means applied magnetic field could promote the forward phase transformation, while in the case of Fe-Pd whose ΔM is negative. That is why the magnetic field will retard the forward transformation in Fe-Pd. It should be emphasized that the magnetic field effect on the phase transformation is very small in both NiMnGa and Fe-Pd alloys because of small magnetization difference between martensite and austenite phase.

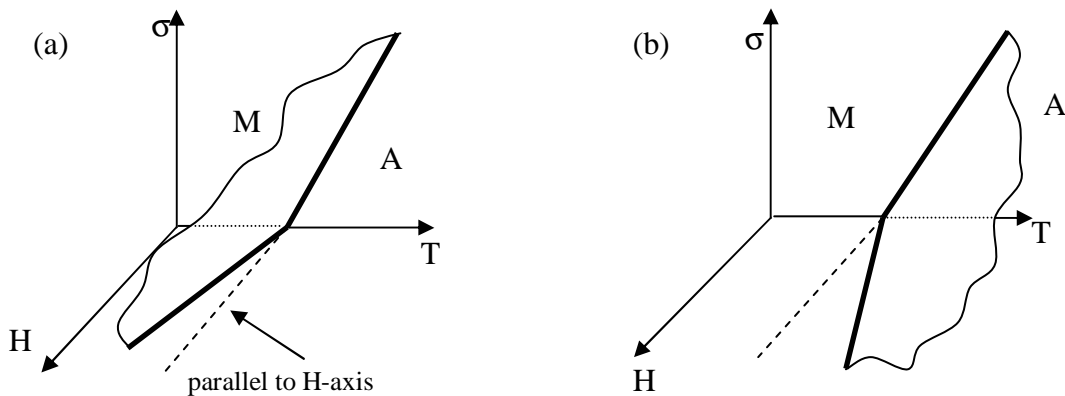


Figure 6 Schematic phase transformation diagram of a FSMA under stress (σ), temperature (T) and magnetic field (H); (a) Fe-Pd and (b) NiMnGa

The smaller susceptibility in the martensite phase (as shown in Fig. 5) reflects a possibility that the magnetic domain wall movement is not so easy as that in the austenite state. The domain wall movement requires a large energy dissipation. The magnetization in a small field appears rather to be achieved by the rotation of magnetization vectors. This corresponds to the difficulty of domain wall movement, which is inherent in the martensite structure consisting of small BCVs. In order to move, a magnetic domain wall must sweep the interfaces between BCVs. Rotation of the magnetization vector is more easily achieved. Since this process involves practically no energy dissipation, the magnetization curve should have small hysteresis, in accordance with the present experiment.

As shown in the previous, the movement of interfaces between BCVs involves large energy dissipation: When a unit area of an interface moves by unit distance, $k = 2\text{MPa} = 2 \times 10^6 \text{ J/m}^3$ is dissipated. The magnetic hysteresis is small in Fe-Pd and, thus, only a small fraction of magnetic work is dissipated. However, even under the unrealistic assumption that

all the work is used to move the interfaces of BCVs, it can be shown that changes in variant fractions and resulting strain are negligibly small. W_M , supplied by the magnetic field (H) can be calculated when Fe-Pd is magnetized to saturation (M_S),

$$W_M = \int_0^{M_S} H dM, \quad (28)$$

where M is the magnetization. Reading $M_S (= 1.25 \times 10^6 \text{ A/m})$ in Fig. 5 and integrating the above expression graphically using Fig. 5, $W_M = 6.6 \times 10^4 \text{ J/m}^3$ can be obtained.

The analytical study in Section 2 shows that when the fractions of three BCVs change, the strain is produced. This work implies that when the magnitude of f_i^* describing changes in the fractions of BCVs is small, the energy given by Eq (20) is dissipated. For a rough estimate, $f_2^* = 0$ was used. Then,

$$\delta W_D = k \left(\left| \delta f_1^* \right| \right). \quad (29)$$

Equating W_D with $W_M (= 6.6 \times 10^4 \text{ J/m}^3)$ and using the frictional stress of $k = 2 \times 10^6 \text{ J/m}^3$, we obtain

$$\left| f_1^* \right| = 3.3 \times 10^{-2}. \quad (30)$$

This means that changes in the fractions of BCVs are extremely small when a magnetic field is applied.

The energy dissipation plays an essential role in the above discussion. Only the difference of input energy (such as a magnetic field) and the energy dissipated can be utilized to supply the work for an Fe-Pd based actuator. This means that Fe-Pd cannot be used as an effective actuator, if a pure and direct effect of a magnetic field (i.e. applying uniform field) on variant changes or on the transformation temperature is to be utilized. However, if a large force, produced by a non-uniform distribution of a magnetic field, is used, we may attain sufficient energy for actuation. For example, consider an Fe-Pd sheet in austenite martensite state, clamped at one end and hanging a weight downwards at the other end. If a magnetic field, which becomes stronger upwards, is applied to the Fe-Pd sheet, a magnetic force acts on the sheet upwards, resulting in a bending moment, which causes stress in the sheet. As a result, the sheet will bend up and raise the weight. The sheet is strained by martensite variant changes. Similar deformation is obtained for Fe-Pd in an austenite state and stress-induced transformation attains the deformation¹. In these cases, the designing geometry of a Fe-Pd actuator-magnetic field set-up is more critical. A part of the work supplied through a magnetic field by an electric source is, of course, dissipated. However, the energy dissipated can be supplied by a proper arrangement of a set-up and a sufficiently strong power source. It is noted that the existence of energy dissipation accompanies hysteresis in a strain-magnetic field relationship. Stress induced transformation from austenite to martensite in Fe-Pd involves less energy dissipation. Thus, the exploration of this process, by properly choosing an alloy composition and temperature, is better suited for designing a reversible actuator based on Fe-Pd system.

4. SUMMARY

A micromechanics approach is proposed to calculate the stress-strain relationship of a polycrystalline Fe-Pd ferromagnetic shape memory alloy. It is modeled as consisting of spherical grains, which are grouped according to their orientations with respect to the loading axis. Therefore, the internal stress and elastic energy are accumulated as straining proceeds due to the strain differences between differently oriented grains, using the mean field method. It has been shown that the maximum strain is different for tension and compression. The energy dissipation of the interface movement is also considered and it is estimated based on dislocation theory. Furthermore, a stress-magnetic field-temperature phase transformation diagram was presented as a key performance diagram to FSMA actuator designs.. Although the magnetic field induced phase transformation and martensite variant change are very small, the alloy still

can be utilized as a new actuator material by the hybrid mechanism: the magnetic field gradient induced force (or moment), force induced stress-induced martensitic transformation which leads to large deformation. This mechanism is based on the large magnetization value of Fe-Pd and magnetic field gradient. Moreover, the actuation based on the hybrid mechanism is reversible and very fast¹.

ACKNOWLEDGEMENTS

We are grateful to Professor Mori for his stimulating discussions and help on the micromechanical modeling. This study was supported by DARPA-ONR contract (N-00014-00-1-0520). Dr. E. Garcia of DARPA and Dr. R. Barsoum of ONR are the program monitors. Further support was given by a NEDO grant on Smart Materials where Dr. A. Sakamoto is the program monitor.

REFERENCE

1. Y. Liang, H. Kato and M. Taya, "Bending of Fe-30at.%Pd ferromagnetic shape memory alloy by a magnetic field", *Proc. Plasticity '00:8th Int. Symp. Plasticity and Current Applications, Whistler, Canada*, pp.193-195, 2000.
2. Y. Liang, H. Kato, M. Taya and T. Mori, "Straining of Ni-23Mn-27Ga by martensitic transformation under stress and magnetic fields", *Scripta Mat.* **45/5**, pp 569-574, 2001.
3. S.J. Murray, M. Farinelli, C. Kantner, J.K. Huang, S.M. Allen and R.C. O'Handley, "Field-induced strain under load in NiMnGa magnetic shape memory materials", *J. Appl. Phys.*, **83**, pp.7297-7299, 1998.
4. R.D. James, R. Tickle and M. Wuttig, "Large field-induced strains in ferromagnetic shape memory materials", *Mater. Sci. Eng.*, **A273**, pp.320-325, 1999.
5. K. Ullakko, J.K. Huang, V.V.Kokorin and R.C. O'Handley, "Magnetically controlled shape memory effect in Ni₂MnGa intermetallics", *Scripta Mat.*, **36**, p.1133-1138, 1997.
6. H. Kato, Y. Liang and M. Taya, "Stress-induced FCC/FCT phase transformation in Fe-Pd alloy", *Scripta Mat.*, **46/6**, pp.471-475, 2002.
7. H. Kato, T. Wada, Y. Liang, T. Tagawa, M. Taya and T. Mori, "Martensite Structure in Polycrystalline Fe-Pd", to appear in *Mater. Sci. Eng. A*.
8. T. Mori and K. Tanaka, "Average stress in matrix and average elastic energy of materials with misfitting inclusions", *Acta Metall.*, **21**, pp.571-574, 1973.
9. L. M. Brown, "Back stress, image stress and work hardening", *Acta metall.*, **21**, pp.879-885, 1973.
10. Y. Liang; T. Mori; M. Taya, "Micromechanics of stress-induced martensitic transformation in mono- and polycrystalline shape memory alloys; Ni-Ti", *Advanced Materials for the 21st Century: The 1999 Julia R. Weertman Symposium*, pp.385-396, 1999 *TMS Fall Meeting in Cincinnati, OH, USA.*, Oct. 31-Nov.4, 1999.
11. T. Mura, "Isotropic inclusions", *Micromechanics of Defects in Solids*, pp.79, Martinus Nijhoff, 1982.
12. E. Kuramoto, Y. Aono, Y. Kitajima, K. Maeda and S. Takeuchi, *Phil. Mag. A*, **39**, 717(1979).
13. R. Oshima, "Successive martensitic transformations in Fe-Pd alloys", *Scripta Mat.*, **15**, pp.829-833, 1981.
14. P.J. Webster, K.R.A. Ziebeck, S.L. Town and M.S. Peak, "Magnetic order and phase transformation in Ni₂MnGa", *Phil. Mag. B*, **49**, pp.295-310, 1984.
15. K. Ullakko, J. K. Huang, C. Kantner and R.C. O'Handley, "Large magnetic-field-induced strains in Ni₂MnGa single crystals", *Appl. Phys. Lett.*, **69**, p.1966-1968, 1996.